Chem

CellPress

Article

Mapping out the Degree of Freedom of Hosted Enzymes in Confined Spatial Environments

By virtue of the atomic resolution of the SDSL-EPR technique and the on-demand COF syntheses, we show unambiguously that the degree of freedom of the encapsulated enzymes inside the nanopore varied along with the confined spatial environments. Increasing the hydrophilicity in the isoreticular COFs resulted in the accommodated enzyme with decreasing degrees of freedom and, consequently, lower reactivity. The developed structure-activity relationships are expected to be leveraged to tailor host materials for achieving more efficient formulations.

Qi Sun, Yanxiong Pan, Xiaoliang Wang, ..., Briana Aguila, Zhongyu Yang, Shengqian Ma

zhongyu.yang@ndsu.edu (Z.Y.)
sqma@usf.edu (S.M.)

HIGHLIGHTS

The combination of SDSL-EPR and COFs to understand enzymes' behavior in a confined space

Spatial environments affect the degree of freedom of the encapsulated enzyme

Increasing the host hydrophilicity results in a more constrained conformation of lysozyme

Retained inherent enzyme flexibility to maintain the overall catalytic function

Sun et al., Chem 5, 3184–3195
December 12, 2019
https://doi.org/10.1016/j.chempr.2019.10.002

Chem

CellPress

Article

Mapping out the Degree of Freedom of Hosted Enzymes in Confined Spatial Environments

Qi Sun,[1,3,4] Yanxiong Pan,[2,4] Xiaoliang Wang,[1] Hui Li,[2] Jasmin Farmakes,[2] Briana Aguila,[1] Zhongyu Yang,[2,*] and Shengqian Ma[1,5,*]

SUMMARY

The integration of enzymes with solid materials is crucial for promoting their industrialization. Understanding the enzyme behavior upon association within a confined space, though of fundamental importance for biocomposite development, remains a persistent, unresolved challenge. Here, we present a comprehensive elucidation of the spatial environment's impact on hosted enzymes' degree of freedom and, consequently, their accompanying reactivity. Site-directed spin labeling in combination with electron paramagnetic resonance spectroscopy allows the direct detection of host-guest interactions at atomic resolution, while the tailorable synthesis of covalent organic frameworks (COFs) enables an evaluation of factors affecting such interactions. Specifically, lysozyme is found to be more constrained and less active along with increasing hydrophilicity of the COFs. These results support the establishment of a connection between the hydrophilicity of the spatial environment and the resulting biocomposites' reactivity, enabling the prediction of the performance of unknown biocomposites. This study provides a unique insight into the mechanistic pathways underpinning biocatalysis.

INTRODUCTION

With most practical applications of porous materials reliant on specific interactions with guest molecules that are based on the host-guest interaction, understanding this is a necessity to interpret the properties of existing ones and, in turn, inform the development of better host materials with a specific function.[1] Host-guest interactions have been tailored and investigated extensively by dialing in the desired function,[2–4] but information pertaining to such communications is often phenomenological and is usually extracted from indirect methods associated with line shifts, widths, and/or intensities variation derived from spectroscopy such as Fourier transform infrared (FTIR) spectroscopy. This information proved to be incomplete for elucidating mechanisms underlying function, which often rely on conformational flexibility and spatial arrangement such as for biomolecules.[5,6] Therefore, the design of composite materials relies mainly on laborious and time-consuming trial-and-error experiments. A correlation developed based on experimentally determined structure-property relationships to guide the design of efficient formulations would be ideal; however, both technology and materials innovations are needed.

Enzymes are linear sequences of amino acids that fold to give intricate structures with specific catalytically active sites, producing highly selective products with accelerated reaction rates.[7] Enzyme conformational dynamics play critical roles in

The Bigger Picture

The understanding of spatial enzyme arrangement upon association with porous materials in a confined space is essential for biocomposite development for numerous applications in the field of catalysis, medicine, and separations. In confined environments, surface properties, such as wettability, play a significant role in addition to geometric features. This work demonstrates how the combination of the site-directed spin labeling (SDSL)-electron paramagnetic resonance (EPR) technique and the tunable COF syntheses offers opportunities for building an atomic-level picture of the interactions between the host materials and biomolecules. We establish that increasing the host-material hydrophilicity results in a more constrained conformation of lysozyme and thus its decreased activity. The developed structure-performance descriptors have provided direct shreds of evidence that the conservation of the inherent flexibility is essential to maintain the overall enzyme catalytic function, which also helps improve our understanding of critical cellular mechanisms.

molecular recognition and regulation of the activity.[8] Immobilization of enzymes on confined surfaces is essential for numerous applications of modern protein engineering with optimum performance in the fields of catalysis, separations, and medicine.[9–19] Although the impact of the host material on the enzymatic performance of the resulting biocomposites can be inferred from the divergent outcomes, direct detection of the changing degree of freedom of the enzyme along with the varied pore chemistry of the host materials and the consequent enzymatic performance has been lacking, with structure-activity relationships yet to be established. The reason for this is due in part to that traditional host materials, such as silica and active carbon, are unable to independently fine-tune their pore geometries and chemical functionalities, thereby compromising comparative studies between the individual parameters and the performance of the resultant biocomposites. In addition, a simple variation of functional groups can only allow the pores to access a few discrete chemical states engendered by the host-guest interactions rather than a continuum of states with which a potential guest can match.[20] These barriers can be overcome with the advent of chemistry that allows reticulating molecules into extended frameworks, wherein the pores of the materials can be chemically and geometrically modified to direct the uptake of a target guest molecule.[21] Covalent organic frameworks (COFs) are such a type of porous material, which can be readily engineered to deploy a periodic array of channels that are accessible to guest sorption and can be modified in size, shape, and chemical function to optimize mass-transfer rates and host-guest recognition.[22–36] Moreover, advances in techniques are noteworthy as site-directed spin labeling (SDSL), in combination with electron paramagnetic resonance (EPR) spectroscopy, has proven to be unique for characterizing protein topography, local and global structure, and dynamics regardless of complexities caused by enzyme-matrix signals and/or enzyme-matrix interactions.[37–46] Accordingly, the application of SDSL-EPR for mapping the host-guest interactions of the enzymes within various functional COF pores may be able to answer key questions about the impact of a confined spatial environment on the degree of freedom of the infiltrated enzyme and thereby the accompanying reactivity. These results are also anticipated to offer unique insight into the chemistry of the bespoke host environments in the COFs.

Herein, we report on the enzyme spatial arrangement with respect to the confining pore environments informed by SDSL-EPR. Three carefully chosen isoreticular COFs with different hydrophilicity were initially synthesized and analyzed to determine the correlation between the pore chemical environment and the degree of freedom changes of the hosted enzymes, as well as their subsequent catalytic performance. According to these results, a simple model to represent in terms of hydrophilicity of the host materials and the activities of the infiltrated enzymes was developed. To verify the connection, we used a multivariate (MTV) strategy, by which multiple functional groups can be introduced into one COF material without altering the underlying topology,[47] finding that it is possible to predict the enzymatic activity of the resulting biocomposites for the unknown specific linker ratio with different hydrophilicities. The ability to characterize the degree of freedom changes of the encapsulated enzymes in isoreticular structures by SDSL-EPR and the extracted atomic-level information provides fundamental insights into the relationship between the pore environment and host-guest interactions. The structure-activity relationships derived from these results were thus leveraged to tailor host materials for achieving more efficient formulations. Our results also highlight that COFs are an excellent platform for providing structural insight into the reactivity of the encapsulated guests and are therefore crucial materials for guiding the design of novel composite materials.

[1]Department of Chemistry, University of South Florida, 4202 East Fowler Avenue, Tampa, FL 33620, USA

[2]Department of Chemistry and Biochemistry, North Dakota State University, 1340 Administration Avenue, Fargo, ND 58102, USA

[3]Key Laboratory of Biomass Chemical Engineering, College of Chemical and Biological Engineering, Zhejiang University, Hangzhou, Zhejiang 310027, China

[4]These authors contributed equally

[5]Lead Contact

*Correspondence: zhongyu.yang@ndsu.edu (Z.Y.), sqma@usf.edu (S.M.)

https://doi.org/10.1016/j.chempr.2019.10.002

RESULTS

Biocomposites Synthesis and Characterization

To carry out this study, we first selected a COF prototype for enzyme encapsulation. Previous work has established that the COF, TPB-DMTP-COF, synthesized by the condensation of 2,5-imethoxyterephthalaldehyde (DMTA) and 1,3,5-tris(4-aminophenyl)-benzene (TPB), can be used as an excellent material platform for guest encapsulation, as well as for functional development, due to its high crystallinity, large mesoporous channels (3.3 nm), together with its ultrastability toward a wide range of conditions (hereafter abbreviated as COF-OMe).[48] To better understand the pore environment and its effect on the mobility change of the infiltrated enzymes and their following catalytic properties, we chose to probe the impact of the hydrophilicity of the host materials on the reactivity of the resulting biocomposites because of the well-recognized experimental evidence from literature, including our work.[49,50] Such that, the –OMe group in the linker was replaced with a –OH or –ONa group to yield the COFs denoted as COF-OH and COF-ONa, respectively, with hydrophilicities that follow the trend COF-ONa > COF-OH > COF-OMe (Figure 1A). The COF materials reported herein were generated in accord with the isoreticular principle: when functional groups are introduced to the linkers, the overall lattice structure is unperturbed. Detailed procedures for the synthesis of the COFs have been presented in the Supplemental Information. We selected lysozyme as an enzyme to study. This was not only due to its size fitness with the pore aperture of the selected COFs, which can be confined but not constricted within the COF pore channels, but also because of the well-established SDSL technique for lysozyme, being able to map the host-guest interactions by EPR spectroscopy.[51–53] Furthermore, lysozyme is a ubiquitous enzyme with a number of applications due to its efficiency to cleave the 1,4-glycosidic bond, which compromises the integrity of bacterial cell walls, causing lysis of the bacteria.[54]

To immobilize the enzyme, the COFs were immersed in a lysozyme solution of 4-(2-hydroxyethyl)-1-piperazineethanesulfonic acid (HEPES) buffer (25 mM, pH 7.43) at room temperature. The resultant biocomposites were collected by centrifugation, followed by subsequent washing and drying, affording the composites denoted as lyz@COF-OMe, lyz@COF-OH, and lyz@COF-OMe. The uptake capacities of lysozyme by the COFs were evaluated using ultraviolet-visible (UV-vis) spectroscopy by detecting the concentration of lysozyme in the original solution as well as the combination of the supernatant and washing solutions after immobilization (see details in the Supplemental Information). A loading of 0.5, 0.49, and 0.44 mg mg^{-1} was achieved for COF-OMe, COF-OH, and COF-ONa, respectively, after 24 h (Table S1). Both the crystallinity and morphology of the COFs are preserved after the infiltration of lysozyme, as revealed in the powder X-ray diffraction (PXRD) patterns (Figure 1B) and scanning electron microscopy (SEM) images (Figures S1–S3). FTIR spectra of the biocomposites were also indicative of the encapsulation of lysozyme into the COFs, with the appearance of a peak at around 1,648 cm^{-1} that is ascribed to the amide groups of the enzyme (Figure S4).[49] The successful immobilization of the enzyme in the COFs was further confirmed by the increased N content in the resulting biocomposites, as revealed by the elemental analysis (Table S2). To determine the distribution of lysozyme in the resultant composites, fluorescent probe fluorescein isothiocyanate (FITC) was used to label the enzyme molecules. From the confocal laser scanning microscopy (CLSM), it can be observed that FITC-lysozyme (green) is present throughout the resulting biocomposites, indicating that lysozyme is uniformly inside the COFs (Figure 1C). Their discrepancy in fluorescence intensities can be ascribed to the different thicknesses of the biocomposites in the detected area. To discriminate the location of the enzyme after association with the COFs,

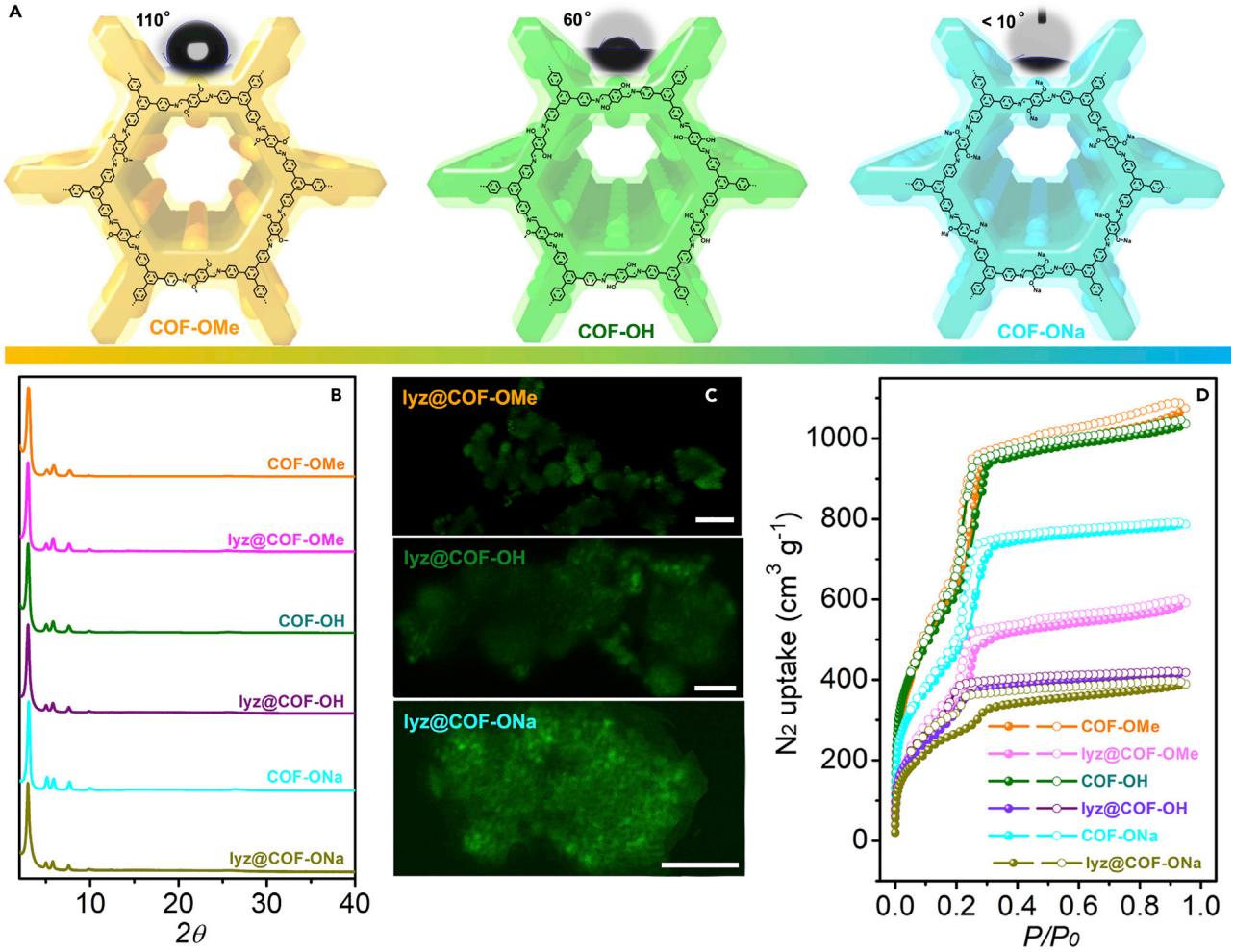

Figure 1. Graphic View and Characterization of the COF Materials and Corresponding Biocomposites

(A) Graphic view and the structure of the COF materials. Inset shows a photograph of a water droplet on the pellet disk made from the corresponding COF.

(B) Normalized PXRD patterns.

(C) Confocal microscopy image of lyz@COFs where lysozyme was labeled with fluorescein isothiocyanate (FITC). Scale bar, 10 μm.

(D) N_2 sorption isotherms collected at 77 K.

See also Figures S1–S9 and Tables S1 and S2.

we exposed the resulting biocomposites to urea aqueous solution, a protein-unfolding chemical. It is shown that only a tiny sharp peak in the mobile component assignable to protein unfolding was detected for the COF-based biocomposite after being treated with urea, while most of the structure of the enzyme was retained. We assume that the sharp component is likely caused by the enzyme adsorbed on the COF surface being unfolded by urea, whereas the steric hindrance of the COF channels prevents the enzyme hosted in the pores from unfolding (Figure S5). To further validate that the vast majority of the enzyme molecules are situated in the pore channels, probe accessibility were evaluated, which showed that the reactivity of the large molecule of cholesteryl chloroformate to the enzyme in lyz@COF-OMe was significantly restricted, yet it had little influence on the reactivity of the small molecule of benzoyl chloride (see details in the Supplemental Information). N_2 sorption isotherms measured at 77 K revealed that the Brunauer-Emmett-Teller (BET) surface area decreased from 1,941 to 1,028 $m^2\ g^{-1}$ for COF-OMe, 1,897 to 951 $m^2\ g^{-1}$ for

COF-OH, and 1,453 to 784 m^2 g^{-1} for COF-ONa, after association with lysozyme (Figures 1D and S6).

Mapping the Degree of Freedom of Lysozyme Housed in COFs with Various Hydrophilicities

After confirming the successful encapsulation of lysozyme into the pores of the COFs, we proceeded to investigate whether there is any spatial arrangement difference along with the varied pore environments by SDSL-EPR. To accomplish this, the recombinant T4 phage lysozyme (T4L) was used instead of the commercial lysozyme (T4L@COFs), wherein six cysteine mutants were introduced individually, covering most regions of the enzyme (Figure 2A), thereby enabling the mapping of the protein topology and determining structural changes after immobilization. The working principle of SDSL is that a protein site of interest is mutated to a cysteine, followed by attaching a stable nitroxyl moiety to form a spin-label sidechain, designated R1 (Figure 2B),[55,56] such that only the dynamics of the R1 sidechain are recorded by the EPR, whereas the interferences from the background materials are ignored.[51–53] To probe the backbone dynamics of each labeled site after association with the COFs, we employed continuous wave EPR in HEPES buffer. Due to the hyperfine splitting, we observed three regions for all of the collected spectra, and each region can be resolved into two spectral components, assignable to spin labels with restricted and/or immobilized and unrestricted or mobile motion (hereafter abbreviated as "im" and "m," respectively; see detailed definition in Figure 2C). These differences stem from the fact that the enzymatic regions exposed to solvents are more dynamic than those associated with the host materials, thereby allowing for the determination of the existence of host-guest interactions as well as the resulting enzyme orientation. Given the sensitivity of the low field region of EPR spectroscopy, we selected this region for more in-depth analyses. To quantify each component, we started to fit the resulting spectra with the established algorithm (see Supplemental Information). Significant differences in EPR signals were detected for the enzyme associated with various COF materials. Among the three biocomposites tested, only the spectrum for T4L@COF-OMe fits well with the established model, which assumes that only the rate and order of the motion of the spin label contribute to the spectra (Figures 2C and 2D). These results indicate that no strong interaction exists between the enzyme and COF-OMe, and the enzyme retains its dynamic flexibility after encapsulation. However, obviously distorted fittings were found for the data acquired from COF-OH and COF-ONa using the model above. We attributed such distortion to the spin-exchange narrowing, which was also supported by the appearance of a strong and symmetric peak at the centerline of the nitroxide spectrum (Figure 2D).[57–59] We reasoned that those spin labels are in very close proximity with the COF pore surfaces, facilitating the communication between the conjugated COF skeletons and the enzyme molecules and thereby leading to the occurrence of the spin-exchange narrowing.

To quantify the extent of such exchange narrowing, some spectral variables were first defined. Given that exchange narrowing results in a symmetric central peak, the ratio of the positive and negative peak intensity (I_{cp} and I_{cn}, respectively; Figure 3A) of the centerline can be used to assess the extent of exchange narrowing, with an I_{cp}/I_{cn} ratio of 1 for a pure exchange narrowing. Detailed analyses of each mutant after association with the various COF materials are shown in Figure 3B, wherein the parameter ranges that do not encounter exchange narrowing are highlighted in gray. It was found that with respect to T4L@COF-OMe, the values of all the mutants are sites within the range of the gray area. By contrast, for T4L@COF-OH, there are two labeled sites (65 and 72) way below the gray area, indicative of the

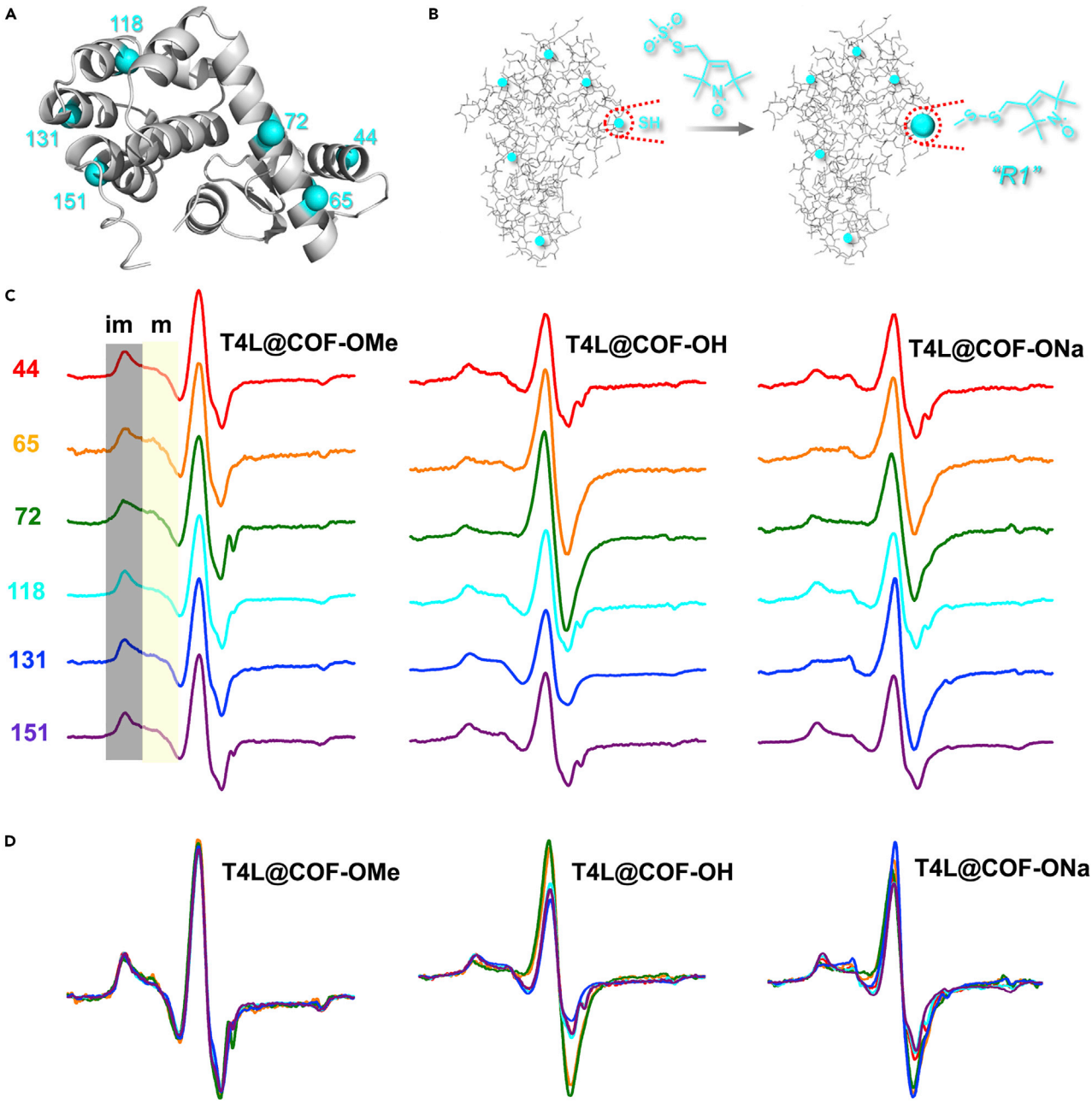

Figure 2. Spin-Labeled Sites and EPR Spectra

(A) Cartoon structure of T4L, showing spin-labeled mutated sites studied in this work.

(B) Reaction of a thiol-containing protein with a sulfhydryl-specific nitroxide reagent generates a disulfide-linked nitroxide side chain (R1).

(C) The EPR spectra of all labeled sites after association with COF-OMe, COF-OH, and COF-ONa, respectively. Gray and light yellow shades labeled with "im" and "m" represent the immobile and mobile spectral components, respectively.

(D) The corresponding overlapped EPR spectra shown in (C).

occurrence of exchange narrowing. Therefore, it can be inferred that sites 65 and 72 tightly contact with the inner wall of the COF-OH channel; interestingly, in regard to COF-ONa, only sites 118 and 151 show I_{cp}/I_{cn} ratios within or close to the gray areas; the other four labeled sites are suggested to have strong host-guest interactions as judged by the exchange narrowing. To validate the aforementioned results, another

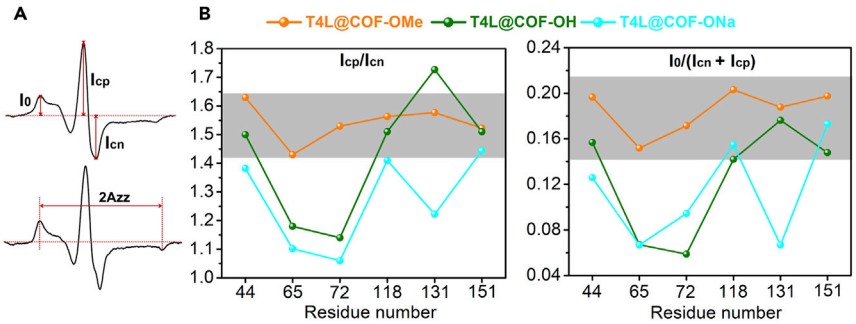

Figure 3. Spectral Variables Definition, Qualification of Spin-Exchange Narrowing, and Proposed Host-Guest Interactions

(A) Definitions of the three variables relevant to spin-exchange narrowing and illustration of measuring the key parameter (A_{zz}) associated with the hydrophilicity of the immobile component of each labeled site.

(B) Quantitative description of the extent of spin-exchange narrowing using the ratio of the positive and negative peaks of the centerline (I_{cp}/I_{cn}) and the ratio of the amplitude of the low-field peak and that of the centerline peak ($I_0/(I_{cp}+I_{cn})$). Gray areas indicate typical parameter regions where no spin-exchange narrowing occurs, and lines are guidelines for the eyes.

parameter for describing the extent of exchange narrowing may be necessary. Given the fact that if the exchange narrowing occurred, the intensity of other peaks in relation to the centerline will be weakened; therefore, the relative ratio of $I_0/(I_{cp}+I_{cn})$ can also be used to assess the extent of exchange narrowing, wherein I_0 refers to the intensity of the low-field peak (Figure 3B). The trend profiles derived from the calculated $I_0/(I_{cp}+I_{cn})$ values are in good accordance with that from I_{cp}/I_{cn}, thus corroborating the accuracy of the results.

Based on these analyses, we proposed the spatial arrangement of the enzyme in the COFs (Figure 3B). Taking into account the confinement effect in the COFs, the enzyme is only allowed to penetrate the COF channels along its long axis. Given the absence of exchange narrowing between the hosted enzyme and COF-OMe, it is believed that all the labeled sites have a similar possibility to contact with the COF. Whereas in T4L@COF-OH, the sites 65 and 72 are more inclined to contact with the channel walls in comparison to other sites, and this number was further increased to four in the case of COF-ONa, wherein the sites 65, 72, 44, and 131 exhibited strong interaction with the COF, suggesting that the enzyme is more constrained in the order of T4L@COF-ONa > T4L@COF-OH > T4L@COF-OMe (Figure S7). These results implied that the hydrophilicity of the bulk material has a great impact on the degree of freedom of the hosted enzyme. To give a better connection between the bulk material and the pore channel's wettability, we measured the local hydrophobicity of the labeled site, given the sensitivity of the hyperfine splitting of a continuous wave EPR spectrum toward the varied hydrophilicities. The A_{zz} value, which is defined in Figure 3A, can be used to quantify the hydrophilicity, with a higher value indicating a lower hydrophobicity. As shown in Table S3, the average A_{zz} values for the enzyme hosted in COF-OMe, COF-OH, and COF-ONa are 34.93, 35.44, and 35.52 G, respectively (Figure S8). This trend is in excellent agreement with the expected hydrophobicity of the COF channels. These results imply how leveraging the pore environment engineering to alter the host-guest interactions may lead to the design of new biocomposites for advanced applications. In this case, modifying the hydrophilicity in related materials could afford control over their binding affinity for the specific sites and potentially enable the manipulation of the performance of the resulting biocomposites.

Enzymatic Activity Assay

Given the differences, we surmised that varying the pore environment of the host material would lead to divergent reaction outcomes of the accommodated enzyme. In view of that lysozyme is known for catalyzing the cleavage of the 1,4-glycosidic bond, hydrolysis activities toward chitosan of the lyz@COF samples were investigated by tracking the *N*-acetylglucosamine amount via a potassium ferricyanide measurement of UV-vis absorbance at 420 nm (no leaching was observed for any of the lyz@COF catalysts; see details in Supplemental Experimental Procedures). While the surface areas, pore sizes, and enzyme loading amounts of these three biocomposites are relatively similar, their activities are dramatically different, decreasing in the order lyz@COF-OMe > lyz@COF-OH > lyz@COF-ONa. Specifically, lyz@COF-ONa is almost inactive, while the *N*-acetylglucosamine yield catalyzed by lyz@COF-OMe is about two times that by lyz@COF-OH. We verified that the discrepancy in enzymatic activity came from the different host-guest interaction but instead as a result of the substrate diffusional limitations by measuring isotherms of enzyme adsorption and corresponding catalytic performance (Figure S9). The reactivity of the immobilized enzyme changing along with the varied host-guest interactions can be rationalized based on the proposed mechanism for the enzymatic catalysis whereby the intrinsic flexibility of the enzyme, especially near the active site, is important for facilitating the binding of substrates and the overall enzyme catalytic function.[60] Therefore, the less constrained enzyme with a higher degree of freedom is expected to give superior catalytic efficiency. This was also proven by the following experimental evidence that the rates for lyz@COFs in the hydrolysis of chitosan are all lower than the free lysozyme in solution, which may be caused by the restricted freedom after association with host materials, mass transport limitations, or the nonoptimized interface between the COFs and lysozyme. It is worth mentioning that these issues could be overcome in the future by modifying the linkers for COF synthesis to tailor the pore aperture size and the pore environment.

Structure-Activity Relationship Establishment

These findings suggest the connection between the hydrophilicity of host materials and the activity of the accommodated lysozyme; increasing the host-material hydrophilicity results in the more constrained conformation of the enzyme and thus decreased activity. This brings about the question: is there any possibility to envisage such an interaction according to the hydrophilicity of the host material employed so that one can predict the catalytic performance of the enzyme therein? To further address this question, we applied the MTV strategy to manipulate the pore hydrophilicity finely and to investigate whether it is possible to predict the performance of the resulting biocomposites for the unknown specific linker ratio with different hydrophilicities. To target this, a three-component condensation system was introduced with equal moles of 2,5-dihydroxyterephthalaldehyde and 2,5-dimethoxyterephthalaldehyde as edge units to synthesize a COF with a –OMe and –OH group ratio of one, denoted as COF-OMe-OH (Figures S10–S12). With the hydrophilicity difference between COF-OMe and COF-OH, we surmised that the interaction between the enzyme and COF-OMe-OH should fall in between them. Indeed, EPR spectra revealed that the trend of interaction with the COF for each mutant is in good accordance with that predicted, with exchange narrowing occurrences in two sites, 65 and 72. This was further intensified in COF-OMe-2OH with increased hydrophilicity, wherein the –OH and –OMe group ratio is two, yet they are weaker than those in COF-OH (Figures S13–S17). Impressively, the catalytic assays revealed that the reactivity of lyz@COF-OMe-OH and lyz@COF-OMe-2OH were within the range of lyz@COF-OMe and lyz@COF-OH. These results demonstrate the validity of this connection between the host-material hydrophilicity and the degree of

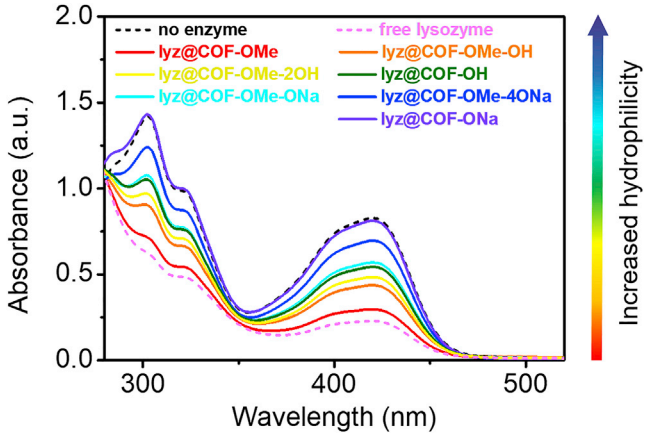

Figure 4. Catalytic Assay

UV-vis spectra for various catalysts in the hydrolysis of chitosan in 0.1 M acetate buffer. A decrease in the intensity at 420 nm relates to an increase in the activity of the enzyme. See also Figures S10–S27 and Tables S3–S5.

freedom of the hosted enzyme, which is expected to be used to predict their reactivity in an isoreticular COF in terms of hydrophilicity. To further prove the applicability of this model, two more materials with increased hydrophilicities were synthesized, COF-OMe-ONa and COF-OMe-4ONa (Figures S18–S21). After association with lysozyme, the resulting enzymatic activities are well consistent with the hydrophilicity of the host materials, giving reactivity decreasing in the order lyz@COF-ONa < lyz@COF-OMe-4ONa < lyz@COF-OMe-ONa < lyz@COF-OH < lyz@COF-OMe-2OH < lyz@COF-OMe-OH < lyz@COF-OMe (Figure 4). Taken together, we can now conclude that functionalization of the struts with hydrophilic elements directly translates into the interaction of the enzyme with the COF, and the extent of this effect is proportional to the hydrophilicity, as well as the density of functional groups that are installed. Advantageously, in light of the fact that the value of host-guest interaction energy could be varied continuously, quantification of their behavior can provide a precise understanding of the interplay between the host material and the enzyme, underpinning the reactivity of the resulting biocomposites.

After verifying the connection between the host materials' hydrophilicity on the reactivity of the infiltrated enzymes, the question we ask here is if it can be leveraged for guiding the design of biocomposites with better performance. To answer this, we paired 2,5-dimethylterephthalaldehyde with TPB to synthesize another isoreticular COF material to COF-OMe but with a higher hydrophobicity, denoted as COF-Me (Figures S22–S24). EPR profiles reveal that the average Azz value of COF-Me after association with T4L is 34.48 G, lower than that of COF-OMe (34.93 G; Figure S25; Table S3), supporting that COF-Me provides a more hydrophobic environment. The spectral resolution indicated that enzymes in COF-Me have a higher percentage of the mobile component of each labeled site than that in COF-OMe (see second row from the bottom of Tables S4 and S5; Figure S26), validating that they have a higher degree of freedom in COF-Me. Indeed, lyz@COF-Me outperformed lyz@COF-OMe in the hydrolysis of chitosan (Figure S27).

DISCUSSION

In summary, by virtue of the atomic resolution of the SDSL-EPR technique and the on-demand COF syntheses, we showed unambiguously that the enzymes inside

the nanopore align with the confined spatial environments, which vary the host-guest interactions and thus the divergent reaction outcomes. For lysozyme, we showed that increasing the hydrophilicity in the isoreticular COFs resulted in the accommodated enzyme with decreasing degrees of freedom, which have deleterious effects on the reactivity. The identification of bulk materials' wettability linking to the mobility and reactivity of the hosted enzyme provides robust structure-property relationships, and the means to perform inverse biocomposite design. Furthermore, given that enzymes inside the nanopore are likely to mimic more faithfully the tightly packed environment inside cells, our results might be used to sample other biological confined reactions. We expect the research presented to also have a broad impact in efficiently mapping the relevant host-guest interactions that directly link to the property.

EXPERIMENTAL PROCEDURES

Materials

Commercially available reagents were purchased in high purity and used without purification. The synthetic procedures of other monomers used for the COF synthesis were detailed in the Material Synthesis section (Supplemental Information), with the purity verified by the NMR technique (Figure S28).

Biocomposite Synthesis and Enzymatic Activity Assay

The procedures for biocomposite synthesis and enzymatic activity assay are detailed in the Supplemental Information (Figures S29–S32).

Characterization

Powder X-ray diffraction (PXRD) data were collected on a Bruker AXS D8 Advance A25 Powder X-ray diffractometer (40 kV, 40 mA) using Cu Kα (λ = 1.5406 Å) radiation. The gas adsorption isotherms were collected on a surface area analyzer, ASAP 2020. The N_2 sorption isotherms were measured at 77 K using a liquid N_2 bath. Scanning electron microscopy (SEM) images were performed on a Hitachi SU 8000. Infrared (IR) spectra were recorded on a Nicolet Impact 410 FTIR spectrometer. ^{1}H NMR spectra were recorded on a Bruker Avance-400 (400 MHz) spectrometer. Chemical shifts are expressed in ppm downfield from TMS at δ = 0 ppm, and *J* values are given in Hz. Photographs of water drops on the surface of the samples in the pressed pellet form were measured with SL200KB (USA KNO Industry Co.), equipped with a CCD camera. The confocal laser scanning microscopy (CLSM) data were collected on a Leica SP5 under an excitation λ_{ex} = 488 nm and long pass emission at λ_{em} = 500–550 nm. For EPR measurements, samples were transferred into a borosilicate capillary tube (0.70 mm i.d./1.00 mm o.d.; Wilmad Labglass, Inc.). CHNS elemental analyses were performed on a Perkin-Elmer series II CHNS analyzer 2400. A Varian E-109 spectrometer equipped with a cavity resonator was used for the acquisition. All continuous wave (CW) EPR spectra were obtained with an observe power of 200 mW, a modulation frequency of 100 kHz, and a modulation amplitude of 1.0 G (Figure S33).

SUPPLEMENTAL INFORMATION

Supplemental Information can be found online at https://doi.org/10.1016/j.chempr.2019.10.002.

ACKNOWLEDGMENTS

This work was supported by the US National Science Foundation (DMR-1352065). Z.Y. acknowledges the financial support from NSF ND EPSCoR seed award (no. FAR0030347).

AUTHOR CONTRIBUTIONS

Q.S., Y.Z., and S.M. conceived and designed the research. Q.S. and X.W. performed the synthesis and carried out the catalytic assay. Y.P., H.L., and J.F. prepared all spin-labeled enzyme samples and performed EPR data acquisition and analysis. All authors participated in drafting the paper and gave approval to the final version of the manuscript.

DECLARATION OF INTERESTS

The authors declare no competing interests.

Received: June 26, 2019
Revised: July 23, 2019
Accepted: October 1, 2019
Published: October 28, 2019

REFERENCES AND NOTES

1. Ma, X., and Zhao, Y. (2015). Biomedical applications of supramolecular systems based on host-guest interactions. Chem. Rev. *115*, 7794–7839.

2. Chen, B., Xiang, S., and Qian, G. (2010). Metal-organic frameworks with functional pores for recognition of small molecules. Acc. Chem. Res. *43*, 1115–1124.

3. Cooke, G., and Rotello, V.M. (2002). Methods of modulating hydrogen bonded interactions in synthetic host-guest systems. Chem. Soc. Rev. *31*, 275–286.

4. Dong, Z., Sun, Y., Chu, J., Zhang, X., and Deng, H. (2017). Multivariate metal-organic frameworks for dialing-in the binding and programming the release of drug molecules. J. Am. Chem. Soc. *139*, 14209–14216.

5. Houk, K.N., Leach, A.G., Kim, S.P., and Zhang, X. (2003). Binding affinities of host-guest, protein-ligand, and protein-transition-state complexes. Angew. Chem. Int. Ed. Engl. *42*, 4872–4897.

6. Hanefeld, U., Gardossi, L., and Magner, E. (2009). Understanding enzyme immobilization. Chem. Soc. Rev. *38*, 453–468.

7. Schmid, A., Dordick, J.S., Hauer, B., Kiener, A., Wubbolts, M., and Witholt, B. (2001). Industrial biocatalysis today and tomorrow. Nature *409*, 258–268.

8. Van Meervelt, V., Soskine, M., Singh, S., Schuurman-Wolters, G.K., Wijma, H.J., Poolman, B., and Maglia, G. (2017). Real-time conformational changes and controlled orientation of native proteins inside a protein nanoreactor. J. Am. Chem. Soc. *139*, 18640–18646.

9. Dicosimo, R., McAuliffe, J., Poulose, A.J., and Bohlmann, G. (2013). Industrial use of immobilized enzymes. Chem. Soc. Rev. *42*, 6437–6474.

10. Bornscheuer, U.T. (2003). Immobilizing enzymes: how to create more suitable biocatalysts. Angew. Chem. Int. Ed. Engl. *42*, 3336–3337.

11. Sheldon, R.A. (2007). Enzyme immobilization: the quest for optimum performance. Adv. Synth. Catal *349*, 1289–1307.

12. Lian, X., Fang, Y., Joseph, E., Wang, Q., Li, J., Banerjee, S., Lollar, C., Wang, X., and Zhou, H.C. (2017). Enzyme-MOF (metal-organic framework) composites. Chem. Soc. Rev. *46*, 3386–3401.

13. Majewski, M.B., Howarth, A.J., Li, P., Wasielewski, M.R., Hupp, J.T., and Farha, O.K. (2017). Enzyme encapsulation in metal-organic frameworks for applications in catalysis. CrystEngComm. *19*, 4082–4091.

14. Doonan, C., Riccò, R., Liang, K., Bradshaw, D., and Falcaro, P. (2017). Metal-organic frameworks at the biointerface: synthetic strategies and applications. Acc. Chem. Res. *50*, 1423–1432.

15. Gkaniatsou, E., Sicard, C., Ricoux, R., Mahy, J.-P., Steunou, N., and Serre, C. (2017). Metal-organic frameworks: a novel host platform for enzymatic catalysis and detection. Mater. Horiz. *4*, 55–63.

16. Chen, W.-H., Vázquez-González, M., Zoabi, A., Abu-Reziq, R., and Willner, I. (2018). Biocatalytic cascades driven by enzymes encapsulated in metal-organic framework nanoparticles. Nat. Catal. *1*, 689–695.

17. Shieh, F.K., Wang, S.C., Yen, C.I., Wu, C.C., Dutta, S., Chou, L.Y., Morabito, J.V., Hu, P., Hsu, M.H., Wu, K.C., et al. (2015). Imparting functionality to biocatalysts via embedding enzymes into nanoporous materials by a de novo approach: size-selective sheltering of catalase in metal-organic framework microcrystals. J. Am. Chem. Soc. *137*, 4276–4279.

18. An, H., Li, M., Gao, J., Zhang, Z., Ma, S., and Chen, Y. (2019). Incorporation of biomolecules in metal-organic frameworks for advanced applications. Coord. Chem. Rev. *384*, 90–106.

19. Li, P., Modica, J., Howarth, A., Vargas, L.E., Moghadam, P., Snurr, R., Mrksich, M., Hupp, J., and Farha, O. (2016). Toward design rules for enzyme immobilization in hierarchical mesoporous metal-organic frameworks. Chem *1*, 154–169.

20. Matsuzaki, S., Arai, T., Ikemoto, K., Inokuma, Y., and Fujita, M. (2014). Networked-cage microcrystals for evaluation of host-guest interactions. J. Am. Chem. Soc. *136*, 17899–17901.

21. Diercks, C.S., and Yaghi, O.M. (2017). The atom, the molecule, and the covalent organic framework. Science *355*, eaal1585.

22. Feng, X., Ding, X., and Jiang, D. (2012). Covalent organic frameworks. Chem. Soc. Rev. *41*, 6010–6022.

23. Ding, S.Y., and Wang, W. (2013). Covalent organic frameworks (COFs): from design to applications. Chem. Soc. Rev. *42*, 548–568.

24. Jin, Y., Hu, Y., and Zhang, W. (2017). Tessellated multiparous two-dimensional covalent organic frameworks. Nat. Rev. Chem. *1*, s41570–s41617.

25. Bisbey, R.P., and Dichtel, W.R. (2017). Covalent organic frameworks as a platform for multidimensional polymerization. ACS Cent. Sci. *3*, 533–543.

26. Beuerle, F., and Gole, B. (2018). Covalent organic frameworks and cage compounds: design and applications of polymeric and discrete organic scaffolds. Angew. Chem. Int. Ed. Engl. *57*, 4850–4878.

27. Song, Y., Sun, Q., Aguila, B., and Ma, S. (2019). Opportunities of covalent organic frameworks for advanced applications. Adv. Sci. *6*, 1801410.

28. Kandambeth, S., Dey, K., and Banerjee, R. (2019). Covalent organic frameworks: chemistry beyond the structure. J. Am. Chem. Soc. *141*, 1807–1822.

29. Lohse, M.S., and Bein, T. (2018). Covalent organic frameworks: structures, synthesis, and applications. Adv. Funct. Mater *28*, 1705553.

30. Han, X., Huang, J., Yuan, C., Liu, Y., and Cui, Y. (2018). Chiral 3D covalent organic frameworks for high performance liquid chromatographic enantioseparation. J. Am. Chem. Soc. *140*, 892–895.

31. Fang, Q., Wang, J., Gu, S., Kaspar, R.B., Zhuang, Z., Zheng, J., Guo, H., Qiu, S., and Yan, Y. (2015). 3D porous crystalline polyimide

covalent organic frameworks for drug delivery. J. Am. Chem. Soc. *137*, 8352–8355.

32. Roeser, J., Prill, D., Bojdys, M.J., Fayon, P., Trewin, A., Fitch, A.N., Schmidt, M.U., and Thomas, A. (2017). Anionic silicate organic frameworks constructed from hexacoordinate silicon centres. Nat. Chem. *9*, 977–982.

33. Wang, X., Chen, L., Chong, S.Y., Little, M.A., Wu, Y., Zhu, W.H., Clowes, R., Yan, Y., Zwijnenburg, M.A., Sprick, R.S., et al. (2018). Sulfone-containing covalent organic frameworks for photocatalytic hydrogen evolution from water. Nat. Chem. *10*, 1180–1189.

34. Kandambeth, S., Venkatesh, V.V., Shinde, D.B., Kumari, S., Halder, A., Verma, S., and Banerjee, R. (2015). Self-templated chemically stable hollow spherical covalent organic framework. Nat. Commun. *6*, 6786.

35. Sun, Q., Aguila, B., Lan, P.C., and Ma, S. (2019). Tuning pore heterogeneity in covalent organic frameworks for enhanced enzyme accessibility and resistance against denaturants. Adv. Mater. *31*, 1900008.

36. Peng, Y., Huang, Y., Zhu, Y., Chen, B., Wang, L., Lai, Z., Zhang, Z., Zhao, M., Tan, C., Yang, N., et al. (2017). Ultrathin two-dimensional covalent organic framework nanosheets: preparation and application in highly sensitive and selective DNA detection. J. Am. Chem. Soc. *139*, 8698–8704.

37. Fleissner, M.R., Bridges, M.D., Brooks, E.K., Cascio, D., Kálai, T., Hideg, K., and Hubbell, W.L. (2011). Structure and dynamics of a conformationally constrained nitroxide side chain and applications in EPR spectroscopy. Proc. Natl. Acad. Sci. USA *108*, 16241–16246.

38. Hubbell, W.L., López, C.J., Altenbach, C., and Yang, Z. (2013). Technological advances in site-directed spin labeling of proteins. Curr. Opin. Struct. Biol. *23*, 725–733.

39. Cafiso, D.S. (2014). Identifying and quantitating conformational exchange in membrane proteins using site-directed spin labeling. Acc. Chem. Res. *47*, 3102–3109.

40. McHaourab, H.S., Steed, P.R., and Kazmier, K. (2011). Toward the fourth dimension of membrane protein structure: insight into dynamics from spin-labeling EPR spectroscopy. Structure *19*, 1549–1561.

41. Pan, Y., Neupane, S., Farmakes, J., Bridges, M., Froberg, J., Rao, J., Qian, S.Y., Liu, G., Choi, Y., and Yang, Z. (2017). Probing the structural basis and adsorption mechanism of an enzyme on nano-sized protein carriers. Nanoscale *9*, 3512–3523.

42. Pan, Y., Li, H., Farmakes, J., Xiao, F., Chen, B., Ma, S., and Yang, Z. (2018). How do enzymes orient on metal-organic framework (MOF) surfaces? J. Am. Chem. Soc. *140*, 16032–16036.

43. Huang, Y.W., Lai, Y.C., Tsai, C.J., and Chiang, Y.W. (2011). Mesopores provide an amorphous state suitable for studying biomolecular structures at cryogenic temperatures. Proc. Natl. Acad. Sci. USA *108*, 14145–14150.

44. DeBerg, H.A., Brzovic, P.S., Flynn, G.E., Zagotta, W.N., and Stoll, S. (2016). Structure and energetics of allosteric regulation of HCN2 ion channels by cyclic nucleotides. J. Biol. Chem. *291*, 371–381.

45. Vazquez Reyes, C., Tangprasertchai, N.S., Yogesha, S.D., Nguyen, R.H., Zhang, X., Rajan, R., and Qin, P.Z. (2016). Nucleic acid-dependent conformational changes in CRISPR-Cas9 revealed by site-directed spin labeling. Cell Biochem. Biophys. *75*, 1–8.

46. López, C.J., Fleissner, M.R., Brooks, E.K., and Hubbell, W.L. (2014). Stationary-phase EPR for exploring protein structure, conformation, and dynamics in spin-labeled proteins. Biochemistry *53*, 7067–7075.

47. Deng, H., Doonan, C.J., Furukawa, H., Ferreira, R.B., Towne, J., Knobler, C.B., Wang, B., and Yaghi, O.M. (2010). Multiple functional groups of varying rations in metal-organic frameworks. Science *327*, 846–850.

48. Xu, H., Gao, J., and Jiang, D. (2015). Stable, crystalline, porous, covalent organic frameworks as a platform for chiral organocatalysts. Nat. Chem. *7*, 905–912.

49. Sun, Q., Fu, C.W., Aguila, B., Perman, J.A., Wang, S., Huang, H.Y., Xiao, F.S., and Ma, S. (2018). Pore environment control and enhanced performance of enzymes infiltrated in covalent organic frameworks. J. Am. Chem. Soc. *140*, 984–992.

50. Liang, W., Xu, H., Carraro, F., Maddigan, N.K., Li, Q., Bell, S.G., Huang, D.M., Tarzia, A., Solomon, M.B., Amenitsch, H., et al. (2019). Enhanced activity of enzymes encapsulated in hydrophilic metal organic frameworks. J. Am. Chem. Soc. *141*, 2348–2355.

51. Fleissner, M.R., Cascio, D., and Hubbell, W.L. (2009). Structural origin of weakly ordered nitroxide motion in spin-labeled proteins. Protein Sci. *18*, 893–908.

52. López, C.J., Fleissner, M.R., Guo, Z., Kusnetzow, A.K., and Hubbell, W.L. (2009). Osmolyte perturbation reveals conformational equilibria in spin-labeled proteins. Protein Sci. *18*, 1637–1652.

53. Borbat, P.P., McHaourab, H.S., and Freed, J.H. (2002). Protein structure determination using long-distance constraints from double-quantum coherence ESR: study of T4 lysozyme. J. Am. Chem. Soc. *124*, 5304–5314.

54. Zhang, S., Zheng, Y., An, H., Aguila, B., Yang, C.X., Dong, Y., Xie, W., Cheng, P., Zhang, Z., Chen, Y., et al. (2018). Covalent organic frameworks with chirality enriched by biomolecules for efficient chiral separation. Angew. Chem. Int. Ed. Engl. *57*, 16754–16759.

55. Todd, A.P., Cong, J., Levinthal, F., Levinthal, C., and Hubbell, W.L. (1989). Site-directed mutagenesis of colicin E1 provides specific attachment sites for spin labels whose spectra are sensitive to local conformation. Proteins *6*, 294–305.

56. Fleissner, M.R., Brustad, E.M., Kálai, T., Altenbach, C., Cascio, D., Peters, F.B., Hideg, K., Peuker, S., Schultz, P.G., and Hubbell, W.L. (2009). Site-directed spin labeling of a genetically encoded unnatural amino acid. Proc. Natl. Acad. Sci. USA *106*, 21637–21642.

57. Molin, Y.N., Salikhov, K.M., and Zamaraev, K.I. (1980). Spin Exchange (Springer-Verlag).

58. Chen, M., Margittai, M., Chen, J., and Langen, R. (2007). Investigation of α-synuclein fibril structure by site-directed spin labeling. J. Biol. Chem. *282*, 24970–24979.

59. Margittai, M., and Langen, R. (2004). Template-assisted filament growth by parallel stacking of tau. Proc. Natl. Acad. Sci. USA *101*, 10278–10283.

60. Richard, J.P. (2019). Protein flexibility and stiffness enable efficient enzymatic catalysis. J. Am. Chem. Soc. *141*, 3320–3331.